Generation linewidth of mode-hopping spin torque oscillators

Ezio Iacocca,[1,*] Olle Heinonen,[2] P. K. Muduli,[1,3] and Johan Åkerman[1,4]
[1]*Physics Department, University of Gothenburg, 412 96 Gothenburg, Sweden*
[2]*Materials Science Division, Argonne National Laboratory, Lemont, Illinois 60439, USA*
[3]*Department of Physics, Indian Institute of Technology Delhi, Hauz Khas 110016, New Delhi, India*
[4]*Material Physics, School of ICT, Royal Institute of Technology, Electrum 229, 164 40 Kista, Sweden*
(Received 2 December 2013; revised manuscript received 16 January 2014; published 4 February 2014)

Experiments on spin torque oscillators commonly observe multimode signals. Recent theoretical works have ascribed the multimode signal generation to coupling between energy-separated spin wave modes. Here, we analyze in detail the dynamics generated by such mode coupling. We show analytically that the mode-hopping dynamics broaden the generation linewidth and makes it generally well described by a Voigt line shape. Furthermore, we show that the mode-hopping contribution to the linewidth can dominate, in which case it provides a direct measure of the mode-hopping rate. Due to the thermal drive of mode-hopping events, the mode-hopping rate also provides information on the energy barrier separating modes and temperature-dependent linewidth broadening. Our results are in good agreement with experiments, revealing the physical mechanism behind the linewidth broadening in multimode spin torque oscillators.

DOI: 10.1103/PhysRevB.89.054402 PACS number(s): 85.75.−d, 75.78.Cd, 05.45.−a

I. INTRODUCTION

Nanoscopic excitation of high-amplitude magnetization dynamics has recently emerged due to the discovery of the spin-transfer torque (STT) effect and advances in nanofabrication [1,2]. STT describes the momentum transfer from spin-polarized electrons to a local magnetization and therefore provides a direct coupling between dc charge currents and magnetization dynamics. Depending on external conditions, a rich variety of physical phenomena with technologically interesting outcomes are possible, including different modes of spin wave generation [3–8], vortex gyration [9–12], and the nucleation and manipulation of magnetic droplet solitons [13–16]. Regardless of the particular magnetization dynamics, devices where a stable oscillatory state can be achieved are generally referred to as spin torque oscillators [17,18] (STOs) and are typically composed of two ferromagnetic layers decoupled by a nonmagnetic spacer (although recent studies also report on STOs based on single ferromagnet layers [19]). STOs are engineered to enforce magnetization dynamics in one of the ferromagnetic layers (the "free" layer), whereas the second layer (the "fixed" layer) acts both as a polarizer and a reference to probe the dynamics via magnetoresistive effects [20–25].

STOs have been traditionally regarded as single-mode oscillators [26,27] based on the mode selection imposed by the balance of STT and magnetic damping as well as the survival of the mode with the lowest threshold. However, recent experiments have shown multimode generation in a large variety of geometries [28–30], revealing evidence of mode hopping [31–33], periodic mode transitions [5,7], and even coexistence [8]. Furthermore, such a multimode generation leads to broader linewidths ascribed to the reduction of the magnetization dynamics coherence. In order to understand the underlying physics of these observations, a multimodal theoretical description is required.

A first step towards this goal was recently proposed [32–34] by extending the Slavin-Tiberkevich auto-oscillator theory [27] for two coupled modes. The general form of such an extension was found to agree with the equations describing multimode ring lasers [35,36] and thus support mode hopping. However, the model equations remained qualitative and their relation to experimental observables was not explored. Here, we investigate multimode STOs with a goal to *quantitatively* describe their generation linewidth and thus provide a direct connection with experimental quantities, revealing the underlying physical mechanism driving the dynamics.

A central result of this paper is the derivation of the expected linewidth of a two-mode oscillator in a mode-hopping regime. We show that the linewidth is enhanced by multimode generation and is described by a Voigt line shape. Mode-hopping events can be described by a Poisson process, providing a purely Lorenztian contribution to the linewidth which dominates at high mode-hopping rates. Such rates are well described by an Arrhenius distribution, providing information on the energy barrier between the modes and furthermore explaining temperature-driven linewidth broadening. The presented results offer means to experimentally access previously unexplored features of STOs and directly connect experiments with parameters in the theory.

II. MULTI-MODE ANALYTICAL FRAMEWORK

The multimode model equations introduced in Ref. [32] originate from first-principle calculations by considering, e.g., two stable modes coupled by scattering processes in a magnon bath [37]. As a consequence, additional damping, torque, and coupling terms arise. Here, we further incorporate thermal fluctuations following the scheme of Ref. [27], where $\tilde{f} = f^R + if^I$ is a Gaussian distributed perturbation with real and imaginary components and second moment given by $\langle \tilde{f}(t)\tilde{f}(t')\rangle = p_i \Delta\omega\delta(t-t')$, where p_i is the power of the ith mode and $\Delta\omega$ is the (linear) STO generation linewidth

*ezio.iacocca@physics.gu.se

derived from the Slavin-Tiberkevich framework. Performing some algebra (Appendix A), the coupled equations can be cast in terms of the variables θ and ψ which map, respectively, the modes' energy and their phase difference onto a two-dimensional phase space

$$\begin{aligned}\dot{\theta} &= \cos\theta\Gamma_G p\frac{1-\sin\theta}{2\omega_1}[\bar{Q}_1-\bar{Q}_0+\xi(\bar{P}_1-\bar{P}_0)]\\ &\quad-\cos\theta\Gamma_G p\frac{1+\sin\theta}{2\omega_2}[\bar{Q}_2-\bar{Q}_0+\xi(\bar{P}_2-\bar{P}_0)]\\ &\quad+K(1-\sin\theta)\sqrt{\frac{\omega_2}{\omega_1}}\cos(\phi_c-\psi)\\ &\quad-K(1+\sin\theta)\sqrt{\frac{\omega_1}{\omega_2}}\cos(\phi_c+\psi)\\ &\quad+\sqrt{\frac{2}{p}}\left[\cos\frac{\theta}{2}\left(f_2^R-f_1^R\right)-\sin\frac{\theta}{2}\left(f_2^R+f_1^R\right)\right],\end{aligned}\tag{1a}$$

$$\begin{aligned}\dot{\psi} &= \frac{pN_0}{2}\left[\frac{1-\sin\theta}{\omega_1}-\frac{1+\sin\theta}{\omega_2}\right]\\ &\quad+K\frac{1-\sin\theta}{\cos\theta}\sqrt{\frac{\omega_2}{\omega_1}}\sin(\phi_c-\psi)\\ &\quad-K\frac{1+\sin\theta}{\cos\theta}\sqrt{\frac{\omega_1}{\omega_2}}\sin(\phi_c+\psi)\\ &\quad+\sqrt{\frac{2}{p}}\left[\frac{\cos\frac{\theta}{2}\left(f_2^I-f_1^I\right)-\sin\frac{\theta}{2}\left(f_2^I+f_1^I\right)}{\cos\theta}\right].\end{aligned}\tag{1b}$$

Here, the total power $p=p_1+p_2$ is enforced to be constant, given that $p_1=p\cos^2(\theta/2+\pi/4)$, $p_2=p\sin^2(\theta/2+\pi/4)$, and the condition $|\theta|\leqslant\pi/2$ is satisfied. The coefficients $\bar{Q}_i$ and $\bar{Q}_0$ are the diagonal and off-diagonal damping terms, whereas $\bar{P}_i$ and $\bar{P}_0$ are the diagonal and off-diagonal STT terms. They are related to the auto-oscillator terms as $\Gamma_+(p_i)=\Gamma_G(1+\bar{Q}_i p_i+\bar{Q}_0 p_j)$ and $\Gamma_-(p_i)=\xi\Gamma_G(1-\bar{P}_i p_i-\bar{P}_0 p_j)$, where i,j are indices for each of the two modes, $\xi=I_{dc}/I_{th}$ is the supercriticality, I_{dc} is the bias current, I_{th} is the threshold current for auto-oscillations, $\Gamma_G=\alpha\omega_o$, α is the Gilbert damping, and ω_o is the ferromagnetic resonance (FMR) frequency. A coupling term is included as a complex factor $Ke^{i\phi_c}$, with amplitude and phase K and ϕ_c, respectively. As we see below, these terms determine the multimode dynamics and impact the generation linewidth.

Despite the algebraic complexity of Eq. (1), two limiting cases are readily obtained when the thermal fluctuations are neglected (Appendix B). A single mode exists when $\theta=\pm\pi/2$ and $K\to 0$, i.e., the coupling between modes is negligible [Fig. 1(a)]. Note that ψ diverges in this limit since a phase difference cannot be defined. From linear stability analysis (Appendix B) we find that the modes are independently stable if $\bar{Q}_i+\xi\bar{P}_i<\bar{Q}_0+\xi\bar{P}_0$. On the other hand, periodic mode transition and coexistence are possible when $K>0$. Linear stability analysis (Appendix B) demonstrates that each scenario depends on the coupling phase ϕ_c, as indicated in Fig. 1(c). Between the two limiting cases described above, near-single modes and coexistence are possible [Fig. 1(b)].

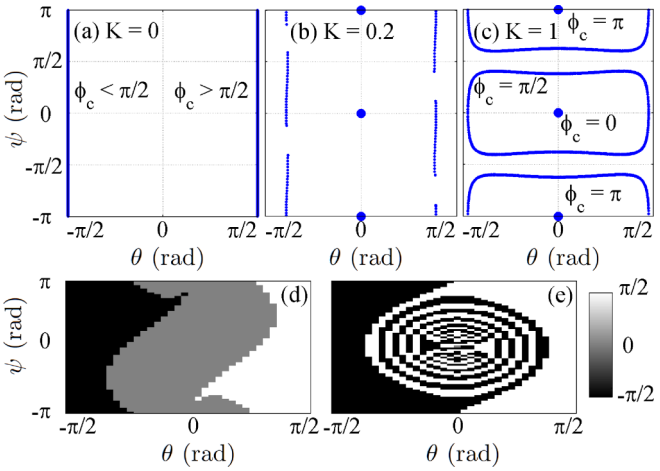

FIG. 1. (Color online) Phase spaces spanned by θ and ψ for (a) $K=0$: single mode; (b) $K=0.2$: near-single modes and co-existence; and (c) $K=1$: coexistence and periodic mode transitions. For the case $K=0.2$, the basins of attraction are shown for (d) $\phi_c=0$ and (e) $\phi_c=\pi/2$. In the latter, the spiral feature is reminiscent of a particle with friction in a double potential well.

The near-single-mode scenario is of particular interest since each mode has a finite energy leading to thermally driven mode hopping, as we show below. Furthermore, the basin of attraction becomes strongly dependent on ϕ_c, as shown in Figs. 1(d) and 1(e) when $\phi_c=0$ and $\phi_c=\pi/2$. In the latter case, the spiral feature is reminiscent of a particle with friction in a double potential well [38], i.e., two stable modes separated by an energy barrier. In the following, we set $\phi_c=\pi/2$ in order to favor a mode-hopping scenario between two near-single modes.

A typical time-trace exhibiting thermally driven mode hopping is shown in Fig. 2(a), where $K=0.3$, and we assume parameters consistent with the STO used in Ref. [33]. Such a device consists of a 4.5-nm-thick Permalloy free layer with saturation magnetization $\mu_o M_S\approx 0.88$ T, exchange length $\lambda_{ex}=5$ nm, and $\alpha=0.01$. An external field $\mu_o H_a=1$ T is applied at 80 deg with respect to the Permalloy film plane. Whereas the current in Ref. [33] was confined to flow perpendicular to the plane by patterning an elliptical 50 nm $\times$ 150 nm nanocontact, we here, for simplicity, assume a circular nanocontact of radius $R_c\approx 40$ nm, which has a similar effective current-carrying area with an assumed supercriticality $\xi\approx 1.1$. In the two-mode oscillator framework, such parameters are mapped to $\omega_o/2\pi=11.94$ GHz, $p\approx 0.017$, $\bar{Q}\approx 4.6\omega$, $\bar{P}\approx\omega$, $\Gamma_G/2\pi\approx 120$ MHz, $N_0/2\pi\omega\approx 68$ GHz, $\omega/2\pi\approx 13.13$ GHz, and $\Delta\omega/2\pi=0.6$ MHz. These parameters agree fairly well with the near-threshold generation of the real device. In order to complete the analytical description, we assume parameters for the off-diagonal terms $\bar{Q}_0=2\bar{Q}$ and $\bar{P}_0=2\bar{P}$, providing stability for both modes.

A particular mode-hopping event is indicated by the black box in Fig. 2(a) and detailed in Fig. 2(b). In this figure, the intrinsic relaxation frequency of the STO is also apparent, related to its strong nonlinear coefficient N_0 (Appendix B). On the other hand, the mechanism for the mode-hopping events can be clearly illustrated in the (θ,ψ) phase space shown

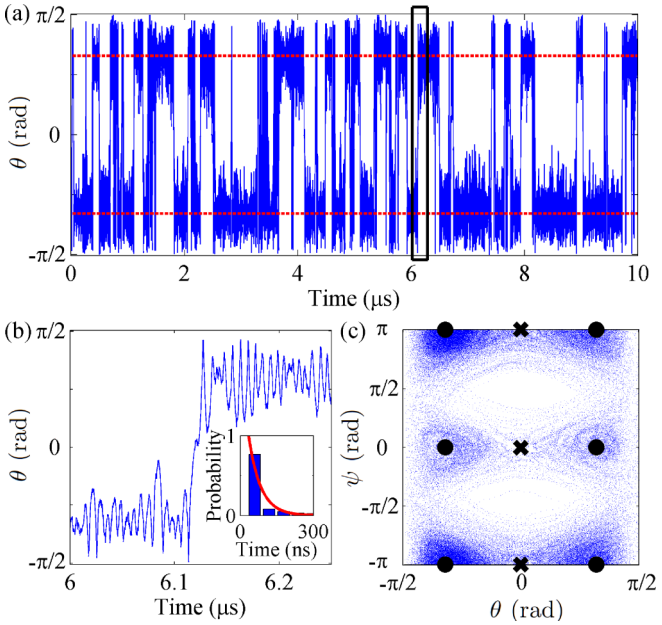

FIG. 2. (Color online) (a) Time trace of θ exhibiting mode-hopping events between $\pm\langle\theta_o\rangle$ (dashed lines, red online). The section in the black box is detailed in panel (b), where the underlying relaxation frequency is observed. The inset shows the exponential distribution of the time difference between mode-hopping events, in agreement with a Poisson process. (c) Phase space of the time trace (a) showing that the stable modes (fixed points indicated by black dots) are thermally driven to mode hop via saddle points (black crosses).

in Fig. 2(c). Here, the hopping between the different stable fixed points (indicated by black dots) occur via saddle points (indicated by black crosses). This picture also agrees with the above-mentioned similarity between this system and a double potential well.

III. GENERATION LINEWIDTH

The generation linewidth of the resulting dynamics can be analytically estimated by means of the autocorrelation function of the two-mode oscillator, defined as

$$\mathcal{K} = \langle [c_1(t) + c_2(t)][c_1^*(t') + c_2^*(t')]\rangle, \tag{2}$$

where $c_i = \sqrt{p_i}e^{i\phi_i}$ is the complex amplitude of each mode, related to its power p_i and phase ϕ_i. By manipulating the phases of each mode, it can be shown that the autocorrelation depends only on the second moment of the phase difference ψ (Appendix C), thus providing a tractable expression for $\mathcal{K}$. Consequently, the problem is reduced to analyzing the thermally induced behavior of ψ.

To proceed, two vastly different time scales are identified: (i) the perturbation introduced by thermal fluctuations and (ii) mode-hopping events. The former has a short time scale and we assume that the perturbation is small. The latter occurs as sharp phase jumps on a longer time scale (Fig. 2) and cannot be analytically obtained from Eq. (1). Consequently, we incorporate such events as an additional phase parametrized as a random train of pulses. In the following we derive the second moment contribution of each fluctuation source.

The perturbations of the phase difference can be estimated from the linearized coupled equations in phase and power—as suggested in Ref. [27]—by assuming a well-defined energy state for each mode, $\langle\theta_o\rangle$, as shown by dashed lines in Fig. 2(a). Performing a lengthy algebraic manipulation (Appendix D), we can express the power and phase fluctuations as the coupled set of equations

$$\dot{\delta p} = C_{pp}\delta p + C_{p\psi}\delta\psi + f_p, \tag{3a}$$

$$\dot{\delta\psi} = C_{\psi p}\delta p + C_{\psi\psi}\delta\psi + f_\psi, \tag{3b}$$

where the coefficients are given in Appendix D, and it is assumed that $p = p_o + \delta p$ and $\psi = \psi_o + \delta\psi$ satisfy the conditions $\delta p \ll p_o$ and $\delta\psi \ll \psi_o$.

In general, Eqs. (3) can be solved by the standard method of variation of parameters, as detailed in Appendix E. Such a solution leads to second moments proportional to exponential functions of $|\tau| = |t' - t|$. By performing a Taylor expansion to second order, the self- and cross-correlation second moments are

$$\langle\psi_i(t)\psi_i(t')\rangle = \gamma_{L,ii}|\tau| + \gamma_{G,ii}|\tau|^2, \tag{4a}$$

$$\frac{\langle\psi_i(t)\psi_j(t')\rangle}{\cos\langle\theta_o\rangle} = \gamma_{L,ij}|\tau| + \gamma_{G,ij}|\tau|^2, \tag{4b}$$

where the coefficients γ_L and γ_G are mode dependent and are generally functions of the coefficients of Eq. (3) (Appendix E).

On the other hand, mode-hopping events can be described by a series of sudden jumps in the phase difference, separated by random, long time intervals. This description is proper for a Poisson process [39], which is only described by its rate, λ. Indeed, the distribution of the relative time between mode-hopping events is numerically found to agree with an exponential distribution, as shown in the inset of Fig. 2(b). Finally, it is known that the second moment of such a process is simply λ, so the phase difference is enhanced by a factor $-\lambda|\tau|$.

By including the two contributions described above into Eq. (2), we obtain the approximate yet insightful form of the autocorrelation

$$\begin{aligned} 2\mathcal{K} \propto\ & (1 - \sin\langle\theta_o\rangle)e^{-\gamma_{L,ii}|\tau|}e^{-\gamma_{G,ii}|\tau|^2}e^{-\lambda|\tau|} \\ & + (1 - \sin\langle\theta_o\rangle)e^{-\gamma_{L,jj}|\tau|}e^{-\gamma_{G,jj}|\tau|^2}e^{-\lambda|\tau|} \\ & + \cos\langle\theta_o\rangle(e^{-\gamma_{L,ij}|\tau|}e^{-\gamma_{G,ij}|\tau|^2})^{\cos\langle\theta_o\rangle}e^{-\lambda|\tau|} \\ & + \cos\langle\theta_o\rangle(e^{-\gamma_{L,ji}|\tau|}e^{-\gamma_{G,ji}|\tau|^2})^{\cos\langle\theta_o\rangle}e^{-\lambda|\tau|}. \end{aligned} \tag{5}$$

Equation (5) is a central result of this paper. Clearly, as the mode-hopping rate λ increases, there will be a crossover to the temporal decay of the correlation dominated by decoherence arising from mode hopping. The resulting line shape is obtained by the Fourier transform of the autocorrelation Eq. (5), from which the linewidth can be extracted. Each term of the right-hand side has a similar form, which, after performing the Fourier transform, leads to a Lorentzian line shape with a linewidth given by $\gamma_{L,ij} + \lambda$, convoluted by a Gaussian line shape with a linewidth given by $4\sqrt{\gamma_{G,ij}\ln 2}$. Such a convolution is defined as a Voigt line shape. Consequently, the general line shape obtained from the Fourier transform of Eq. (5) is expected to be a sum of Voigt functions. Note that the

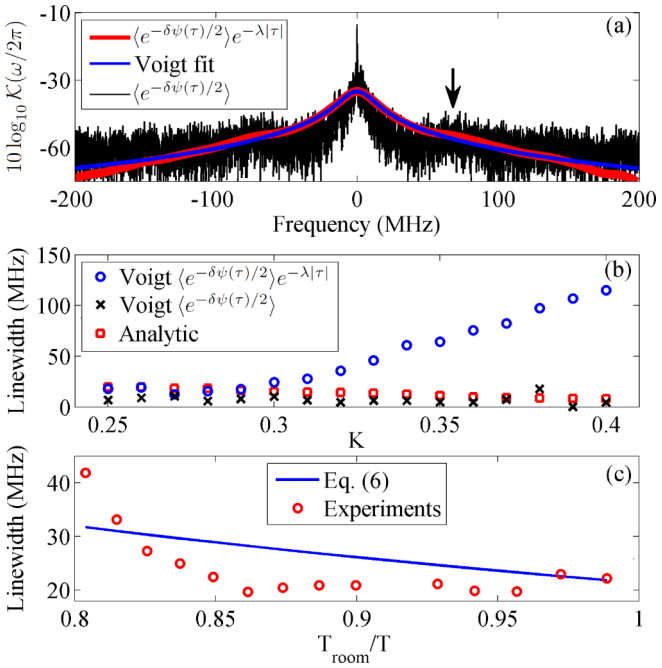

FIG. 3. (Color online) (a) Fourier transform of the autocorrelation calculated from the numerical integration of Eq. (3) (black). Mode-hooping events are included as a Poisson process with a mode-hopping rate calculated from the numerical solution of Eq. (1) (red [gray]). The best Voigt fit is shown in blue (gray). (b) Voigt linewidth as a function of the coupling strength K, obtained from the best fit of the autocorrelation (black) and including mode-hopping events (blue [gray]). The analytical estimate is shown by red (gray) squares. The mode-hopping events dominate the linewidth when $K > 0.3$. (c) Experimentally measured linewdith (red [gray] circles) and linewidth obtained from Eq. (6) (blue [gray] line) with $\Delta E = 52$ meV extracted from a single experimental linewidth data point at 303 K. This simple fit shows a remarkably good agreement with the experimental data trend as well as its magnitude.

mode-hopping rate λ enhances the linewidth of the Lorentzian components, contributing to spectral broadening, as observed experimentally [33]. On the other hand, the Gaussian contribution here arises from the response of Eq. (3), which is found to relax to zero (Appendix E); i.e., the autocorrelation is lost after a finite time, leading to statistically independent modes and thus uncorrelated mode-hopping events. This mechanism has a different physical origin than the Gaussian line shape that arises from a high-temperature limit [27] or $1/f$ noise [40].

IV. NUMERICAL INTEGRATION

Numerically, the line shape predicted from Eq. (5) can be obtained from the autocorrelation of $\delta\psi(t)$ multiplied by the Poisson factor with a mode-hopping rate λ estimated from the time trace of Eq. (1a). Such a line shape is shown in Fig. 3(a) by the red (gray) line for the parameters given earlier. We find the best Voigt fit following the approach of Ref. [41], as shown in the same figure by the blue (gray) line. For the chosen STO parameters, a single Voigt fit provides a good estimate of Eq. (5). The fitting procedure can be repeated as a function of K, from which we obtain the Voigt linewidths, Δf (half width at half maximum), shown in Fig. 3(b) by blue (gray) circles. These numerical results can be quantitatively compared with the analytical estimates from Eqs. (5) and (4). For the chosen parameters, we obtain $\gamma_{G,ii} \to 0$ so that $\gamma_{L,ii}$ provides a good estimate for the linewidth, shown in Fig. 3(b) by red (gray) squares. Clearly, the Voigt fit agrees well with the Lorentzian estimates when $K < 0.3$, suggesting that the linewidth is otherwise dominated by mode-hopping, i.e., $\Delta f \to \lambda$. A second key result of this paper is that the obtained linewidth values *quantitatively* agree with the reference experiment [33] without any fitting parameters, but instead considering the mode hopping as the physical mechanism behind linewidth broadening.

To further test the analytical estimates, we fit the spectrum of the phase difference autocorrelation shown by black lines in Fig. 3(a). Multiple Voigt functions can be identified in this case, in agreement with Eq. (5). In particular, there is a narrow peak consistent with $\gamma_{L,21} \approx \gamma_{G,21} \to 0$. Note that sidebands corresponding to the oscillatory relaxation of the system are observed at about ± 80 MHz (indicated by an arrow), which, together with the large fluctuations, allow us to reliably fit only two Voigt functions. Independently of these difficulties, the wider Voigt linewidth [black marks in Fig. 3(b)] is observed to follow the analytical trend, confirming that the linewidth enhancement is due to mode-hopping events.

The linewidth enhancement is consistent with the experimental observations close to a mode transition, indicating that the mode coupling increases in such a regime. Consequently, the linewidth provides a direct measure of λ. Assuming an Arrhenius distribution for the mode-hopping rate, it is thus possible to experimentally obtain information about the energy barrier, ΔE, between two near-single modes, e.g., as a function of the current,

$$\Delta E(I_{dc}) = k_B T \log \frac{f_a}{\lambda}, \tag{6}$$

where k_B is the Boltzmann constant, T is the temperature, and we assume that the attempt frequency $f_a = 160$ MHz corresponds to twice the intrinsic relaxation frequency since the phase space is $\pi/2$ periodic in θ. Equation (6) reveals that an exponential linewidth broadening is expected as a function of T^{-1} near a mode transition, in contrast to single-mode predictions [27]. Indeed, by estimating $\Delta E = 52$ meV from a single experimental data point at 303 K (Appendix F), we obtain the correct linewidth trend by simple evaluation of the Arrhenius equation [Fig. 3(c)]. A better fit would involve possible changes in the fixed point position as a function of temperature [42] and temperature dependence of the coupling term [37]. However, these details are outside the scope of the present paper.

In summary, we have presented an analytical description of the generation linewidth of a multimode STO, based on a multimode theory [32–34]. The model equations demonstrate that mode-hopping events can dominate the generation linewidth and thus provide the main mechanism behind linewidth broadening. In particular, our results are in quantitative agreement with current- and temperature-dependent linewidths observed experimentally. Furthermore, we showed that the linewidth is dominated by high mode-hopping rates, providing means to determine the energy barrier separating both modes

and the mechanism behind temperature-dependent linewidth broadening. The presented results open up the possibility to study and determine intrinsic properties of multimode STOs.

ACKNOWLEDGMENTS

Support from the Swedish Research Council (VR), the Swedish Foundation for Strategic Research (SSF), and the Knut and Alice Wallenberg Foundation is gratefully acknowledged. Part of the work was supported by the US Department of Energy, Office of Science, Materials Sciences and Engineering Division.

APPENDIX A: DERIVATION OF THE COUPLED EQUATIONS FROM AUTO-OSCILLATOR THEORY

The auto-oscillator equation [27], taking into account thermal fluctuations and a coupling term to another oscillator, can be written as

$$\dot{c}_i + i\omega_i(|c_i|^2)c_i + [\Gamma_+(|c_i|^2) - \Gamma_-(|c_i|^2)]c_i = \tilde{f}(t) + c_j K e^{i\phi_c}, \tag{A1}$$

where the subscripts i and j identify each oscillator, c is the mode's complex amplitude, and ϕ is the mode's phase. $\omega(|c_i|^2)$, $\Gamma_+(|c_i|^2)$, and $\Gamma_-(|c_i|^2)$ are, respectively, the power-dependent oscillation frequency, damping, and negative damping. The perturbation term $\tilde{f}(t)$ represents thermal fluctuations while the coupling term to the jth mode is parametrized by a strength K and phase ϕ_c. For the multimodal model equations the transformation $\bar{Q}_i^2 = \omega_i|c_i|^2$ is performed under the assumption of conserved total power $p = p_1 + p_2$ [32]. By separating real and imaginary parts of Eq. (A1), four coupled equations are obtained:

$$\dot{Q}_i = Q_i\Gamma_G(\xi - 1) - Q_i\Gamma_G\left[\frac{(\bar{Q}_i + \xi\bar{P}_i)}{\omega_i}Q_i^2 + \frac{(\bar{Q}_0 + \xi\bar{P}_0)}{\omega_j}Q_j^2\right] + Q_j K\sqrt{\frac{\omega_i}{\omega_j}}\cos(\phi_c + \phi_j - \phi_i) + f_i^R, \tag{A2a}$$

$$\dot{\phi}_i = \omega_o + \frac{N Q_i}{\omega_i} + K\frac{Q_j}{Q_i}\sqrt{\frac{\omega_i}{\omega_j}}\sin(\phi_c + \phi_j - \phi_i) + f_i^I. \tag{A2b}$$

Here, $\Gamma_G = \alpha\omega_o$, where α is the Gilbert damping and ω_o is the ferromagnetic resonance frequency (FMR); $\xi = I_{dc}/I_{th}$ is the supercriticality where I_{dc} is the bias currents and I_{th} is the threshold current for auto-oscillations.

Furthermore, energy can be mapped into the variable $|\theta| \leqslant \pi/2$ by the transformations $\bar{Q}_1 = \sqrt{p}\cos(\theta/2 + \pi/4)$ and $\bar{Q}_2 = \sqrt{p}\sin(\theta/2 + \pi/4)$. By scaling Eq. (A2a) by $\sin\theta$ and $\cos\theta$ for each mode, we add Eq. (A2a) to obtain a differential equation for θ, whereas we subtract Eq. (A2b) to obtain a differential equation for the phase difference, $\psi = \phi_2 - \phi_1$.

APPENDIX B: LINEAR STABILITY ANALYSIS OF THE MODEL EQUATIONS

For the linear stability analysis, the Jacobian of the model Equations (1) is calculated. Consequently, the fixed points stability is provided by $s < 1$, where the determinant is

$$s = \frac{J_\theta(\theta) + J_\psi(\psi)}{2} \pm \left[\left(\frac{J_\theta(\theta) - J_\psi(\psi)}{2}\right)^2 + J_\psi(\theta)J_\theta(\psi)\right]^{1/2}. \tag{B1}$$

For the limit $K \to 0$, Eq. (B1) simply reduces to the mode-independent stability conditions $\bar{Q}_i + \xi\bar{P}_i < \bar{Q}_0 + \xi\bar{P}_0$. On the other hand, when $K > 0$ the fixed points are given by $\theta = n\pi$ and $\psi = m\pi$ for $n,m = 0,1,2,\ldots$. The determinant for this case can be written as

$$s = \frac{Y_1 - (-1)^{n+m}2K\beta_1}{2} \pm \sqrt{\frac{Y_1^2}{4} - K^2\beta_2^2 - (-1)^{n+m}Y_2 K\beta_2}, \tag{B2}$$

where we use $Y_1 = \Gamma_G p/2[X_1\omega_1^{-1} - X_2\omega_2^{-1}]$, $X_i = \bar{Q}_i - \bar{Q}_0 + \xi(\bar{P}_i - \bar{P}_0)$, $Y_2 = pN_0/2[\omega_1^{-1} + \omega_2^{-1}]$, $\beta_1 = (a^{-1} + a)\cos\phi_c$, $\beta_2 = (a^{-1} + a)\sin\phi_c$, and $a = \sqrt{\omega_1/\omega_2}$. In general, the stable state is observed to be closely related to the coupling phase, ϕ_c. We can further look into two limiting cases. If $\phi_c = \pi/2$, $\beta_1 = 0$, and $\beta_2 \neq 0$, the determinant of Eq. (B2) can be imaginary or real for even or odd values of $n + m$. Consequently, this case demonstrates the possibility of limit cycles. On the other hand, if $\phi_c = l\pi$ (where $l = 0,1,2,\ldots$), $\beta_1 = (-1)^l(a^{-1} + a)$, and $\beta_2 = 0$, the solutions are always real. Consequently, coexistent states are stable (unstable) if $n + m + l$ is even (odd).

APPENDIX C: DERIVATION OF THE AUTO-CORRELATION FUNCTIONS

The auto-correlation function $\mathcal{K} = \langle[c_1(t) + c_2(t)][c_1^*(t') + c_2^*(t')]\rangle$ can be expanded by mapping the complex amplitudes into the variables θ and ψ. Noting that $c_i = \sqrt{p_i}e^{i\psi_i}$ and introducing the variables $\Psi = \phi_1 + \phi_2$ and $\chi = \theta/2 + \pi/4$, we can expand the complex amplitudes to $c_1 = \sqrt{p}\cos[\chi(t)]e^{i[\Psi(t) - \psi(t)]/2}$ and $c_2 = \sqrt{p}\sin[\chi(t)]e^{i[\Psi(t) + \psi(t)]/2}$. Here, we explicitly write the time dependencies of the variables. It is assumed that the average energy of each mode can be parametrized by $\pm\langle\theta_o\rangle$ so that $\langle\cos[\chi(t)]\rangle = \cos\langle\chi\rangle$ and $\langle\sin[\chi(t)]\rangle = \sin\langle\chi\rangle$. Consequently, the auto-correlation can be expressed as

$$\begin{aligned}\mathcal{K} = {} & p\cos^2\langle\chi\rangle e^{i\Psi/2}\langle e^{-i[\psi(t) - \psi(t')]/2}\rangle \\ & p\sin^2\langle\chi\rangle e^{i\Psi/2}\langle e^{i[\psi(t) - \psi(t')]/2}\rangle \\ & \frac{p}{2}\sin 2\langle\chi\rangle e^{i\Psi/2}\langle e^{-i[\psi(t) + \psi(t')]/2}\rangle \\ & \frac{p}{2}\sin 2\langle\chi\rangle e^{i\Psi/2}\langle e^{i[\psi(t) + \psi(t')]/2}\rangle.\end{aligned} \tag{C1}$$

Expanding the exponential functions then leads to the known property for stochastic functions

$$\langle e^{i\psi(t)}\rangle = e^{-\langle\psi(t)^2\rangle/2}. \tag{C2}$$

Without loss of generality, one can assume $t' = 0$ so that $\langle\psi(t')^2\rangle = \langle\psi(t')\rangle^2$. Consequently, the averages contribute as an additional proportionality constant whereas the line shape originates from the form of the second moment $\langle\psi(t)^2\rangle$. For the purposes of this paper, the latter provides the relevant information on the line shape and linewidth, and thus we neglect the proportionality factors for the analytical discussion in the main text.

APPENDIX D: DERIVATION OF THE COUPLED PERTURBED MODEL EQUATIONS

The short time-scale fluctuations can be obtained by linearizing Eq. (1). This can be achieved directly from Eq. (A2) by expanding the power and phase as $p = p_o + \delta p$ and $\psi = \psi_o + \delta\psi$, where p_o and ψ_o are average operating points. Keeping only the perturbation terms leads to

$$\dot{\delta p} = C_{pp}\delta p + C_{p\psi}\delta\psi + f_p, \tag{D1a}$$

$$\dot{\delta\psi} = C_{\psi p}\delta p + C_{\psi\psi}\delta\psi + f_\psi, \tag{D1b}$$

where the coefficients are given by

$$\begin{aligned} C_{pp} = {} & 2\Gamma_G(\xi - 1) - \frac{p_o}{2}\Gamma_G\frac{(\bar{Q}_1 + \xi\bar{P}_1)}{\omega_1}(1 - \sin\langle\theta_o\rangle)^2 \\ & - \frac{p_o}{2}\Gamma_G\frac{(\bar{Q}_2 + \xi\bar{P}_2)}{\omega_2}(1 + \sin\langle\theta_o\rangle)^2 \\ & - \frac{p_o}{2}\Gamma_G(\bar{Q}_0 + \xi\bar{P}_0)\left(\frac{1}{\omega_1} + \frac{1}{\omega_2}\right)(1 - \sin^2\langle\theta_o\rangle) \\ & + K\cos\langle\theta_o\rangle\left[a\cos(\phi_c + \psi) + \frac{1}{a}\cos(\phi_c - \psi)\right], \end{aligned} \tag{D2a}$$

$$C_{p\psi} = p_o K\cos\langle\theta_o\rangle\left[a\sin(\phi_c + \psi) - \frac{1}{a}\sin(\phi_c - \psi)\right], \tag{D2b}$$

$$f_p = \sqrt{2p_o}\left[\cos\left\langle\frac{\theta_o}{2}\right\rangle(f_2^R + f_1^R) + \sin\left\langle\frac{\theta_o}{2}\right\rangle(f_2^R - f_1^R)\right], \tag{D2c}$$

$$C_{\psi p} = -\frac{N_0}{2}\left[\frac{1 + \sin\langle\theta_o\rangle}{\omega_2} - \frac{1 - \sin\langle\theta_o\rangle}{\omega_1}\right], \tag{D2d}$$

$$\begin{aligned} C_{\psi\psi} = {} & -\frac{K}{\cos\langle\theta_o\rangle}\left[(1 - \sin\langle\theta_o\rangle)\frac{1}{a}\cos(\phi_c - \langle\psi\rangle)\right. \\ & \left. - (1 + \sin\langle\theta_o\rangle)a\cos(\phi_c + \langle\psi\rangle)\right], \end{aligned} \tag{D2e}$$

$$\begin{aligned} f_\psi = {} & \frac{1}{\cos\langle\theta_o\rangle}\sqrt{\frac{2}{p_o}}\left[\cos\left\langle\frac{\theta_o}{2}\right\rangle(f_2^I - f_1^I)\right. \\ & \left. - \sin\left\langle\frac{\theta_o}{2}\right\rangle(f_2^I + f_1^I)\right]. \end{aligned} \tag{D2f}$$

Note that Eqs. (D2e) and (D2f) diverge if $\cos\langle\theta_o\rangle = \pi/2$. Such a divergency is understandable from the fact that a purely single-mode oscillation leads to an ill-defined phase difference.

APPENDIX E: GENERAL SOLUTION OF THE COUPLED PERTURBED MODEL EQUATIONS

The coupled set of Eqs. (3) can be generally solved by the method of variation of parameters. By matrix algebra, one can find the eigenvalues, $\lambda_{\pm,i}$, and the eigenvector matrix elements η_i with inverse matrix components η_i' for each mode and solution. Consequently, we can write the temporal solution for $\psi(t)$ as

$$\begin{aligned} \psi_i(t) = {} & \psi_o + \eta_{12,i}e^{\lambda_{+,i}t}\int_0^t[\eta_{11,i}'e^{-\lambda_{+,i}t'}f_p(t') \\ & + \eta_{21,i}'e^{-\lambda_{+,i}t'}f_\psi(t')]dt' + \eta_{22,i}e^{\lambda_{-,i}t} \\ & \times\int_0^t[\eta_{12,i}'e^{-\lambda_{-,i}t'}f_p(t') + \eta_{22,i}'e^{-\lambda_{-,i}t'}f_\psi(t')]dt'. \end{aligned} \tag{E1}$$

From Eq. (E1) it is possible to obtain the self- and cross-correlation phase difference second moments by simple integration. Noting that

$$\langle f_p(t)f_p(t')\rangle = 4p^2\Delta\omega\delta(t - t'), \tag{E2a}$$

$$\langle f_\psi(t)f_\psi(t')\rangle = \frac{4\Delta\omega}{\cos^2\langle\theta_o\rangle}\delta(t - t'), \tag{E2b}$$

we obtain the second moments as a function of $|\tau| = |t' - t|$

$$\begin{aligned} \langle\psi_i(t)\psi_i(t')\rangle = {} & \frac{A_{ii}}{2\lambda_{+,i}}e^{-\lambda_{+,i}|\tau|} + \frac{B_{ii}}{2\lambda_{-,i}}e^{-\lambda_{-,i}|\tau|} \\ & + C_{ii}\frac{e^{-\lambda_{-,i}|\tau|} + e^{-\lambda_{+,i}|\tau|}}{\lambda_{+,i} + \lambda_{-,i}}, \end{aligned} \tag{E3a}$$

$$\begin{aligned} \frac{\langle\psi_i(t)\psi_j(t')\rangle}{\cos\langle\theta_o\rangle} = {} & \frac{A_{ij}}{\lambda_{+,i} + \lambda_{+,j}}e^{-\lambda_{+,j}|\tau|} + \frac{B_{ij}}{\lambda_{-,i} + \lambda_{-,j}}e^{-\lambda_{-,j}|\tau|} \\ & + \frac{C_{ij}e^{-\lambda_{-,j}|\tau|} + C_{ji}e^{-\lambda_{+,i}|\tau|}}{\lambda_{+,i} + \lambda_{-,j}}, \end{aligned} \tag{E3b}$$

where the coefficients are given by

$$A_{ij} = 4\Delta\omega\eta_{12,i}\eta_{12,j}\left[\eta_{11,i}'\eta_{11,j}'p^2 + \frac{\eta_{21,i}'\eta_{21,j}'}{\cos^2\langle\theta_o\rangle}\right], \tag{E4a}$$

$$B_{ij} = 4\Delta\omega\eta_{22,i}\eta_{22,j}\left[\eta_{12,i}'\eta_{12,j}'p^2 + \frac{\eta_{22,i}'\eta_{22,j}'}{\cos^2\langle\theta_o\rangle}\right], \tag{E4b}$$

$$C_{ij} = 4\Delta\omega\eta_{12,i}\eta_{22,j}\left[\eta_{11,i}'\eta_{12,j}'p^2 + \frac{\eta_{21,i}'\eta_{12,j}'}{\cos^2\langle\theta_o\rangle}\right]. \tag{E4c}$$

The exponential function of Eqs. (E3) can be further expanded to second order in $|\tau|$, from which we obtain the

Lorentzian and Gaussian coefficients

$$2\gamma_{L,ij} = \frac{A_{ij}\lambda_{+,j}}{\lambda_{+,i}+\lambda_{+,j}} + \frac{B_{ij}\lambda_{-,j}}{\lambda_{-,i}+\lambda_{-,j}} + \frac{C_{ij}\lambda_{-,j}+C_{ji}\lambda_{+,i}}{\lambda_{+,i}+\lambda_{-,j}}, \tag{E5a}$$

$$-4\gamma_{G,ij} = \frac{A_{ij}\lambda_{+,j}^2}{\lambda_{+,i}+\lambda_{+,j}} + \frac{B_{ij}\lambda_{-,j}^2}{\lambda_{-,i}+\lambda_{-,j}} + \frac{C_{ij}\lambda_{-,j}^2+C_{ji}\lambda_{+,i}^2}{\lambda_{+,i}+\lambda_{-,j}}. \tag{E5b}$$

APPENDIX F: ESTIMATE OF THE ENERGY BARRIER FROM EXPERIMENTAL DATA

In this section we refer to the experimental results obtained in Ref. [33] for a nanocontact STO. The same reference experiment was used throughout the main text for the analytical and numerical calculations. For our analytical estimate, we assume that the linewidth close to a mode transition can be fully described by the mode-hopping rate. Such an assumption implies that the linewidth "floor" obtained from a single-mode autocorrelation [black marks in Fig. 3(b)] is negligible in the temperature range of the fit [Fig. 3(c)].

In the reference experiment, the linewidth was determined as a function of temperature at a bias current, close to a mode transition of 28.4 mA. For this particular bias current, a linewidth of 22.2 MHz was experimentally measured at 303 K. From this single data point, we attempt to estimate the temperature dependence of the linewidth. Assuming the numerically obtained attempt frequency, $f_a = 160$ MHz, it is possible to estimate the energy barrier $\Delta E \approx 52$ meV at 303 K, using Eq. (6). The same equation can be used to estimate the temperature dependence of the linewidth, shown in Fig. 3(c).

The performed estimate describes semiquantitatively the experimental results and the agreement is remarkably good for such a simple estimation. We stress that a the estimate described above implicitly assumes that the energy barrier is constant as a function of temperature, which can be an oversimplification, as discussed in the main text. Indeed, we observe from experiments that the energy barrier deviates within 30% as a function of temperature. Consequently, careful measurements are needed in order to extract ΔE and λ reliably, but such an approach is well beyond the scope of this paper.

[1] J. C. Slonczewski, J. Magn. Magn. Mater. **159**, L1 (1996).
[2] L. Berger, Phys. Rev. B **54**, 9353 (1996).
[3] J. C. Slonczewski, J. Magn. Magn. Mater. **195**, 261 (1999).
[4] A. Slavin and V. Tiberkevich, Phys. Rev. Lett. **95**, 237201 (2005).
[5] S. Bonetti, V. Tiberkevich, G. Consolo, G. Finocchio, P. Muduli, F. Mancoff, A. Slavin, and J. Åkerman, Phys. Rev. Lett. **105**, 217204 (2010).
[6] M. Madami, S. Bonetti, G. Consolo, S. Tacchi, G. Carlotti, G. Gubbiotti, F. B. Mancoff, M. A. Yar, and J. Åkerman, Nat. Nanotechnol. **6**, 635 (2011).
[7] S. Bonetti, V. Puliafito, G. Consolo, V. S. Tiberkevich, A. N. Slavin, and J. Åkerman, Phys. Rev. B **85**, 174427 (2012).
[8] R. K. Dumas, E. Iacocca, S. Bonetti, S. R. Sani, S. M. Mohseni, A. Eklund, J. Persson, O. Heinonen, and J. Åkerman, Phys. Rev. Lett. **110**, 257202 (2013).
[9] V. Pribiag, I. N. Krivorotov, G. D. Fuchs, P. M. Braganca, O. Ozatay, J. C. Sankey, D. C. Ralph, and R. A. Buhrman, Nat. Phys. **3**, 489 (2007).
[10] T. Devolder, J.-V. Kim, M. Manfrini, W. van Roy, L. Lagae, and C. Chappert, Appl. Phys. Lett. **97**, 072512 (2010).
[11] A. Dussaux, B. Georges, J. Grollier, V. Cros, A. V. Khvalkovskiy, A. Fukushima, M. Konoto, H. Kubota, K. Yakushiji, S. Yuasa, A. K. Zvezdin, K. Ando, and A. Fert, Nat. Commun. **1**, 8 (2010).
[12] S. Petit-Watelot, A. Kim, Joo-Von Ruotolo, R. M. Otxoa, K. Bouzehouane, J. Grollier, A. Vansteenkiste, B. Van de Wiele, V. Cros, and T. Devolder, Nat. Phys. **8**, 682 (2012).
[13] M. A. Hoefer, T. J. Silva, and M. W. Keller, Phys. Rev. B **82**, 054432 (2010).
[14] M. A. Hoefer, M. Sommacal, and T. J. Silva, Phys. Rev. B **85**, 214433 (2012).
[15] S. M. Mohseni, S. R. Sani, J. Persson, T. N. A. Nguyen, S. Chung, Y. Pogoryelov, P. K. Muduli, E. Iacocca, A. Eklund, R. K. Dumas, S. Bonetti, A. Deac, M. A. Hoefer, and J. Åkerman, Science **339**, 1295 (2013).
[16] S. M. Mohseni, S. R. Sani, R. K. Dumas, J. Persson, T. N. Ahn Nguyen, S. Chung, Ye. Pogoryelov, P. K. Muduli, E. Iacocca, A. Eklund, and J. Åkerman, Physica B **435**, 84 (2014).
[17] T. Silva and W. Rippard, J. Magn. Magn. Mater. **320**, 1260 (2008).
[18] D. Ralph and M. Stiles, J. Magn. Magn. Mater. **320**, 1190 (2008).
[19] S. Sani, P. Dürrenfeld, S. Mohseni, S. Chung, and J. Åkerman, IEEE Trans. Magn. **49**, 4331 (2013).
[20] M. N. Baibich, J. M. Broto, A. Fert, F. Nguyen Van Dau, F. Petroff, P. Etienne, G. Creuzet, A. Friederich, and J. Chazelas, Phys. Rev. Lett. **61**, 2472 (1988).
[21] G. Binasch, P. Grünberg, F. Saurenbach, and W. Zinn, Phys. Rev. B **39**, 4828 (1989).
[22] M. Tsoi, A. G. M. Jansen, J. Bass, W.-C. Chiang, M. Seck, V. Tsoi, and P. Wyder, Phys. Rev. Lett. **80**, 4281 (1998).
[23] M. Julliere, Phys. Lett. A **54**, 225 (1975).
[24] S. Yuasa, T. Nagahama, A. Fukushima, Y. Suzuki, and K. Ando, Nat. Mater. **3**, 868 (2004).
[25] D. Houssameddine, S. H. Florez, J. A. Katine, J.-P. Michel, U. Ebels, D. Mauri, O. Ozatay, B. Delaet, B. Viala, L. Folks, B. D. Terris, and M.-C. Cyrille, Appl. Phys. Lett. **93**, 022505 (2008).
[26] S. M. Rezende, F. M. de Aguiar, and A. Azevedo, Phys. Rev. Lett. **94**, 037202 (2005).
[27] A. Slavin and V. Tiberkevich, IEEE Trans. Magn. **45**, 1875 (2009).
[28] S. I. Kiselev, J. C. Sankey, I. N. Krivorotov, N. C. Emley, M. Rinkoski, C. Perez, R. A. Buhrman, and D. C. Ralph, Phys. Rev. Lett. **93**, 036601 (2004).
[29] J. C. Sankey, I. N. Krivorotov, S. I. Kiselev, P. M. Braganca, N. C. Emley, R. A. Buhrman, and D. C. Ralph, Phys. Rev. B **72**, 224427 (2005).
[30] Z. Zeng, K. H. Cheung, H. W. Jiang, I. N. Krivorotov, J. A. Katine, V. Tiberkevich, and A. Slavin, Phys. Rev. B **82**, 100410 (2010).

[31] I. N. Krivorotov, N. C. Emley, R. A. Buhrman, and D. C. Ralph, Phys. Rev. B **77**, 054440 (2008).
[32] P. K. Muduli, O. G. Heinonen, and J. Åkerman, Phys. Rev. Lett. **108**, 207203 (2012).
[33] P. K. Muduli, O. G. Heinonen, and J. Åkerman, Phys. Rev. B **86**, 174408 (2012).
[34] O. Heinonen, P. Muduli, E. Iacocca, and J. Åkerman, IEEE Trans. Magn. **49**, 4398 (2013).
[35] S. Beri, L. Gelens, M. Mestre, G. Van der Sande, G. Verschaffelt, A. Scirè, G. Mezosi, M. Sorel, and J. Danckaert, Phys. Rev. Lett. **101**, 093903 (2008).
[36] G. V. der Sande, L. Gelens, P. Tassin, A. Scir, and J. Danckaert, J. Phys. B **41**, 095402 (2008).
[37] O. Heinonen, Y. Zhou, and D. Li, arXiv:1310.6791.
[38] E. Ott, *Chaos in Dynamical Systems* (Cambridge University Press, Cambridge, 1994).
[39] T. Silva and M. Keller, IEEE Trans. Magn. **46**, 3555 (2010).
[40] M. W. Keller, M. R. Pufall, W. H. Rippard, and T. J. Silva, Phys. Rev. B **82**, 054416 (2010).
[41] Y. Liu, J. Lin, G. Huang, Y. Guo, and C. Duan, J. Opt. Soc. Am. B **18**, 666 (2001).
[42] S. Banerjee, R. Bhattacharya, and C. Chakrabarti, Int. J. Math. Math. Sci. **23**, 435 (2000).